# Fluorescence Quenching of Aromatic Amino Acids by Rhodium Nanoparticles

Elizaveta Demishkevich[1,*], Alexander Zozulya[1], Andrey Zyubin[1], Ivan Lyatun[1], Ilia Samusev[1]

[1] Immanuel Kant Baltic Federal University, A.Nevskogo St. 14, Kaliningrad, Russia, 236016

* Correspondence: ldemishkevich@gmail.com; Tel.: +7-963-2994124;

**Received**: Oct 24, 2024 **Revised**: Dec 02, 2024 **Just Accepted Online**: Dec 13, 2024 **Published**: Xxx



E. Demishkevich, A. Zozulya, A. Zyubin, I. Lyatun, I. Samusev (2024) Fluorescence Quenching of Aromatic Amino Acids by Rhodium Nanoparticles. **Substantia**. *Just Accepted*. DOI: 10.36253/Substantia-3055



## Abstract

In this paper, the fluorescence quenching of the aromatic amino acids tyrosine and tryptophan by rhodium nanoparticles has been investigated. The choice of rhodium nanoparticles was determined by the fact that the plasmonic maximum of the nanoparticles and the absorption range of the amino acids are in the UV. The quenching constants and types of quenching were estimated using Stern-Volmer dependencies. The fluorescence intensity of amino acids was found to decrease with nanoparticle concentration, with different types of quenching observed: tryptophan-nanoparticle system showed static quenching, while dual quenching (static and dynamic) occurred in tyrosine-nanoparticle system. Calculation of parameters of quenching efficiency were done: diffusion coefficient, diffusion rate parameter and quenching activation energy. Opportunities to exploit quenching mechanisms to realise optical sensing effects in UV have been shown.

Keywords: aromatic amino acids, tyrosine, tryptophan, fluorescence spectroscopy.

## Introduction

Fluorescence spectroscopy is actively used to study the structure and dynamics of proteins and other biological macromolecules [1,2]. The intrinsic fluorescence of proteins is due to the presence of aromatic amino acids: tyrosine (Tyr), tryptophan (Trp) and phenylalanine (Phe) [3]. The optical activity of these aromatic amino acids has long been of interest to scientists and has been actively used to study protein aggregation and conformation [4,5]. Trp, Tyr and Phe also play the role of internal fluorescent probes of protein conformation, dynamics and intermolecular interactions [6,7].

The contribution of Phe to protein fluorescence is small due to of its low absorbance and quantum yield [8] Tyr fluorescence in native proteins is often suppressed by energy transfer to Trp, therefore, Tyr is less frequently used for protein studies [9,10]. However, protein

unfolding can lead to partial elimination of Tyr quenching, making it to be a useful indicator for protein conformational changes [11,12].

The possibility of Tyr fluorescence use to monitor conformational changes in proteins that are not detected by Trp fluorescence was investigated by a group of authors Zhdanova et.al. [13] where human and bovine serum albumin were chosen as model objects.

Trp is most often used as a probe because it is the dominant absorber at $\lambda \sim 280$ nm and the emission source at $\lambda \sim 350$ nm [9]. Trp fluorescence has been found to be very sensitive and responsive to changes in its microenvironment. For example, denaturation of bovine serum albumin (BSA) under the action of sodium dodecyl sulfate (SDS) was investigated on the basis of Trp fluorescence quenching [14]. The fluorescence intensity change of free Trp and Trp attached to the membrane of *Escherichia coli* and *Bacillus subtilis* was determined [15]. It is shown that for Trp being in a free state and not attached to the protein, there is no increase in fluorescence intensity. Fluorescence intensity enhancement can be explained by an additional contribution of Trp fluorescence formed when the protein unfolds, breaking the bond attaching Trp to the membrane of the bacterial protein. Studies on the application of metal surfaces and particles to investigate the fluorescence intensity enhancement/quenching are being actively developed and published.

Metal-enhanced fluorescence (MEF) can lead up to 100 times intensity increase due to the plasmon-enhanced local field. Meanwhile, fluorescence emission can be quenched for fluorophores at short distance (<5 nm) from the metal surface or in direct contact with the metal surface, in which the quenching effect overwhelms the enhancement effect. Different mechanisms for the fluorescence enhancement and quenching of metal nanoparticles have been suggested, but the precise mechanism is still unknown due to the complexity of metal–fluorophore interactions [16]. Metal nanostructures can be useful as fluorescence signal amplifiers for DNA detection [17,18]. Traditionally, nanoparticles of noble metals have been synthesized for fluorescence studies of protein compounds [19–24]. However, the development of science indicates the importance of investigating the use of other metals whose application is possible for the UV-range. Suitable metals for UV-range studies are represented by aluminum [25,26], copper [27]. However, there are plenty of works in which it is shown that the presence of oxide film together with high sensitivity to temperature and humidity result in the difficulty of using such metals for work in the UV range [28,29]. The noble metals such as rhodium and platinum are increasingly attracting the attention of scientific groups. Such metals are considered to be perspective for this area due to their characteristics, namely, resistance to environmental conditions, biocompatibility, and absence of oxide film [30]. Platinum nanoparticles (PtNPs) are increasingly used to enhance the capabilities of modern sensor technologies. The use of Pt nanostructures for the implementation of the UV–MEF method has been studied. Akbay et al. studied MEF of nucleic acids using platinum nanostructured substrates [31]. In the presence of Pt nanostructures, guanosine monophosphate exhibited a higher fluorescence intensity compared to control samples on a quartz substrate. An optical sensor was used for determining oxygen concentration based on a Pt(II) complex and silver-coated SiO2 nanoparticles embedded in a sol–gel matrix [32].

Fluorescence quenching is also actively used to investigate the interaction between fluorophore molecules and nanoparticles. For such purposes, already familiar metals, namely gold and silver, are most often used [33]. The hydrophilic ferroferric oxide nanoparticles and hydrophobic nanoparticles were used to study the interaction mechanism of bovine serum albumin. The presence of dynamic quenching with the first type of nanoparticles and static quenching in the second type was determine [34]. AuNP with diameters of 10 nm were used to study the possibility of controlling fluorescence of fluorophores. The authors were able to experimentally quench and enhance Cypate fluorescence by changing the distance between the fluorophore and GNP [35].

The continuous transition from fluorescence enhancement to fluorescence quenching on a single molecule was measured as a function of distance from a laser-irradiated gold nanoparticle [36].

The quenching of chlorophyll fluorescence by silver nanoparticles with different concentrations and diameters was investigated. It was shown that AgNPs strongly reduced the fluorescence intensity of Chl at 678 nm , which depended on the nanoparticle size with an exponential decrease as a function of the nanoparticle diameter. The authors determined that the fluorescence quenching was caused by a dynamic quenching process, the Stern-Folmer constant being linearly dependent on the nanoparticle size [37].

There is a paper describing the interactions of tyrosine, tryptophan and phenylalanine with biologically synthesized silver nanoparticles. The silver nanoparticles have the ability to quench the intrinsic fluorescence of these amino acids through a dynamic quenching process [38]. In such a case, the issues related to the study of fluorescence of analytes using another noble UV-active metal - rhodium are relevant. A literature review revealed the only paper describing the use of rhodium complexes to study the fluorescence quenching of Trp residue in human serum albumin (HSA) [39].

In the present research we have demonstrated the possibility of fluorescence quenching in amino acid-RhNPs systems, which can be considered as a fundamental basis for the creation of new methods based on ultraviolet plasmonics for biophysical matters.

## Materials and methods

### Reagents

The following reagents were used for the experiment: sodium borohydride $NaBH_4$ (LTD "Lenreaktiv", Russia, purity 97,5%), rhodium chloride $RhCl_3$ (LTD "Aurat", Russia, purity 36 %), aromatic amino acids Tyr (Sigma-Aldrich, EU, purity 99%) and Trp (Sigma-Aldrich, EU, purity 99%). Ultrapure water produced by the Direct-Q 3 UV (Merck, Germany) water purification system was used during synthesis.

### RhNPs synthesis

The synthesis was carried out at room temperature. As a first step, 1.26 g of polyvinylpyrrolidone (PvP) (Mw ~ 55,000) was dissolved in 50 mL of water. Then 200 µl of 0.1 M rhodium salt solution was added to 10 ml of PvP solution. Then 400 µl of freshly prepared and cooled 0.1 M sodium borohydride was added dropwise. After adding the total volume of reducing agent, the solution was stirred for half an hour and left for 24 hours. The synthesised solution was brown in colour. After 24 hours, 5 ml of the solution was centrifuged once at 13000 rpm for 30 minutes. The supernatant was removed and the precipitate was diluted (dispersed) to 5 ml with distilled water. Finally, the concentration of the nanoparticles was calculated:

The volume of the nanoparticle was calculated to determine the concentration:

$V_{np} = \frac{4}{3} \cdot \pi \cdot r^3$, where $r$ - nanoparticle radius, $cm^3$ (1)

Then, we calculated the mass of one particle using the value of volume and density of nanoparticle:

$m_{np} = V_{np} \cdot \rho_{Rh}$, where $\rho_{Rh}$- rhodium metal density (12,41 g/$cm^3$).

The number of nanoparticles is then calculated by the ratio of the total mass of recovered rhodium to the mass of one particle. The amount of rhodium substance is equivalent to the amount of rhodium (III) chloride

$N_{np} = \frac{m_{Rh}}{m_{np}}$, where $m_{Rh}$= 2,1 mg.

Next, we found the mole number of nanoparticles through Avogadro's number:

$n_{np} = \frac{N_{Rh}}{N_A}$, where $N_A$= 6,02·10$^{23}$ M$^{-1}$

The nanoparticle concentration was calculated using the formula:

$C_{np} = \frac{n_{np}}{V}$, where V -nanoparticle solution volume, L

The results of calculations are presented in the Table 1:

Table 1. The results of calculation the RhNPs conrentration

| Parament | Value |
|---|---|
| $V_{np}$, cm$^3$ | 6,24·10$^{-16}$ |
| $m_{np}$, g | 7,74·10$^{-15}$ |
| $N_{np}$ | 2,66·10$^{11}$ |
| $n_{np}$, M | 4,42·10$^{-13}$ |
| $C_{np}$, M | 4,17·10$^{-11}$ |

The concentration of synthesized RhNPs was 4,17·10$^{-11}$ M. We obtained lower concentrations of nanoparticles by diluting the initial concentration with distilled water.

**Sample preparation**

Tyr and Trp solutions with a concentration of 10$^{-5}$ M were prepared. The amino acid was mixed with RhNPs of different concentrations in a 4 mL optically transparent quartz cuvette (Q-1 grade) at room temperature and normal pressure. For this purpose, 3 ml of amino acid and 1 ml of RhNPs were added to the cuvette. After adding the RhNPs to the amino acid, the solution was stirred for 15-30 seconds.

**Experiment**

The absorption maxima of each aromatic amino acid were determined using a UV-2600 spectrophotometer (Shimadzu). 3 ml of the amino acid was placed in a cuvette and then placed in the holder of the spectrophotometer. The spectrum was recorded in the range 200 - 500 nm. The baseline of the absorption spectrum of amino acids was recorded after subtracting the absorption spectrum of distilled water. The absorption spectrum of the synthesised NPs was obtained in a similar way.

The average hydrodynamic radius and zeta-potential of RhNPs were determined using a Photocor Compact-Z (Photocorr) dynamic light scattering spectrometer.

The influence of the presence of RhNPs on the fluorescence intensity of aromatic amino acids was investigated using a spectrofluorometer RF-5301PC (Shimadzu). The fluorescence intensity of aromatic amino acids with RhNPs was investigated using excitation wavelengths corresponding to the absorption maxima of aromatic amino acids (280 nm and 275 nm for Trp and Tyr, respectively).

The fluorescence lifetime of aromatic amino acids was measured on a Fluorolog-3 FL3-22 (Horiba Jobin Yvon) using Data Station software. The spectrum of the empty cuvette was used as the decay for each AA + RhNPs sample. A NanoLED pulsed laser diode operating at λ = 284 nm (Horiba Jobin Yvon) with a nanosecond pulse duration of 1.2 ns was used as an excitation source.

## Results and Discussion

The absorption spectra of aromatic amino acids were obtained as a result of the study (Figure 1). The absorption spectra of the amino acids showed two peaks. The peaks at 280 and 220 nm correspond to Trp, whereas the peaks at 275 and 225 nm correspond to Tyr. Unfortunately, the ability to study kinetics using short wavelength excitation near 220 nm is

not currently available worldwide due to the lack of suitable pulsed radiation sources. Therefore, 280 nm and 275 nm, corresponding to the absorption band of the indole ring for Trp and the phenol ring for Tyr, respectively, were chosen as the excitation wavelengths for obtaining fluorescence spectra of amino acids in the presence of RhNPs to further comply with spectral and time-resolved fluorescence studies.

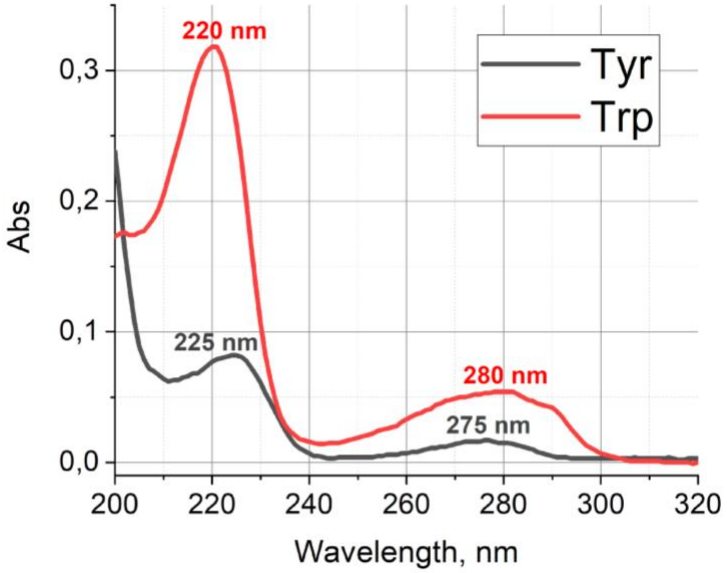


Figure 1. Absorption spectrum of aromatic amino acids: Tyr (gray line), Trp (red line).

Figure 2 shows the absorption spectrum of the synthesized RhNPs. The synthesized RhNPs show a narrow size distribution with an average hydrodynamic radius of 53 nm. The measurement error is 7 per cent (± 4 nm). The plasmonic absorption maximum of the synthesized NPs is in the UV-range at a wavelength of 220 nm. The value of Z-potential = -14.2698019 mV.

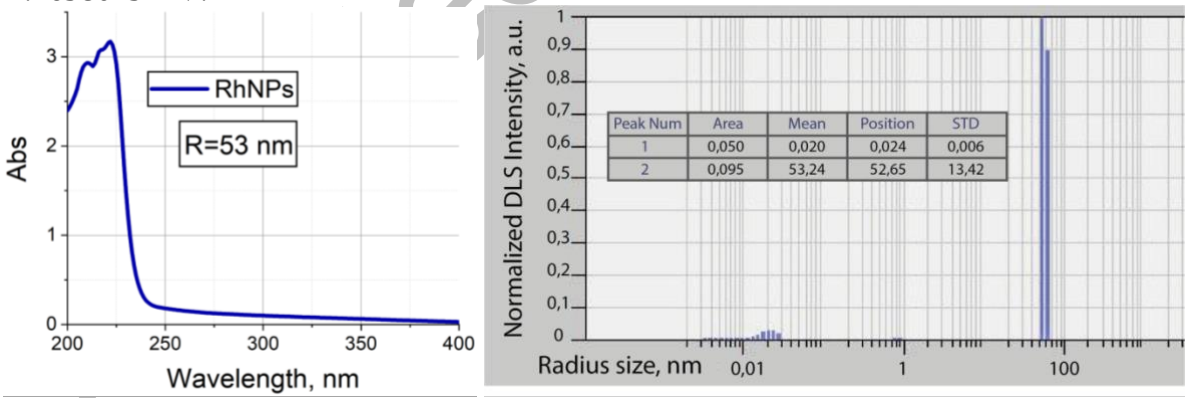


Figure 2. Absorption spectrum (left) and size distribution (right) of RhNPs.

One way to determine the shape of nanoparticles is the absorption spectrum of nanospheres, consistent with literature data [40]. The spectrum of the synthesised nanoparticles by us differs from the spectra of rhodium nanoparticles of other geometries[41–43]**.** The SEM image of the RhNPs was also taken to demonstrate the spherical shape of the synthesised RhNPs (Figure 3). As can be seen in the Figure 3, the RhNPs have a spherical shape. The value of the hydrodynamic radius coincides with the value obtained with the Photocor Compact-Z (Photocorr).

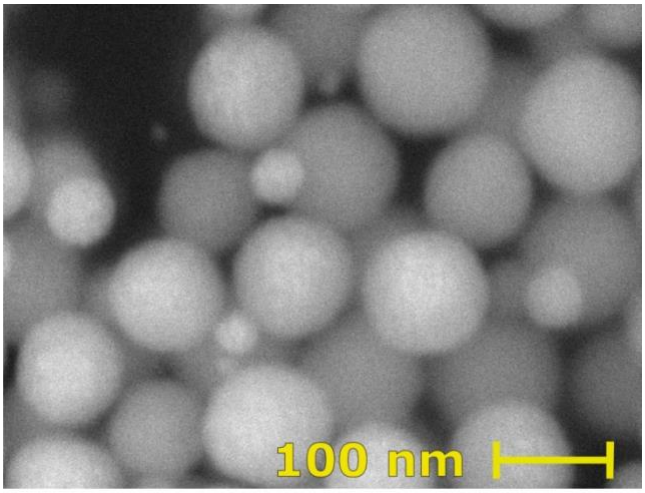


Figure 3. SEM image of synthesized spherical RhNPs.

We obtained the fluorescence and absorption spectra of Trp (Fig.4-5) and Tyr (Fig. 6-7).

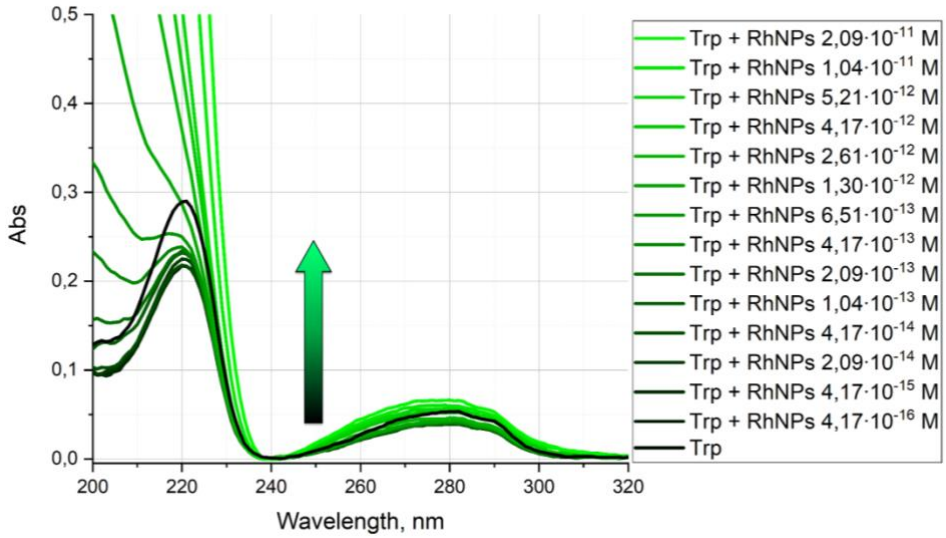


Figure 4. Absorption spectra of Trp with RhNPs of different concentration. Black spectrum - spectrum of Trp without RhNPs, bright green spectrum-spectrum of Trp with RhNPs of highest concentration ( $2{,}09 \cdot 10^{-11}$ M).

As can be seen in Figure 4 the absorption spectrum shows two absorption maxima at 220 nm and maxima at 280 nm which do not change their position. The absorption of Trp

decreases and then increases with increasing concentration of RhNPs.

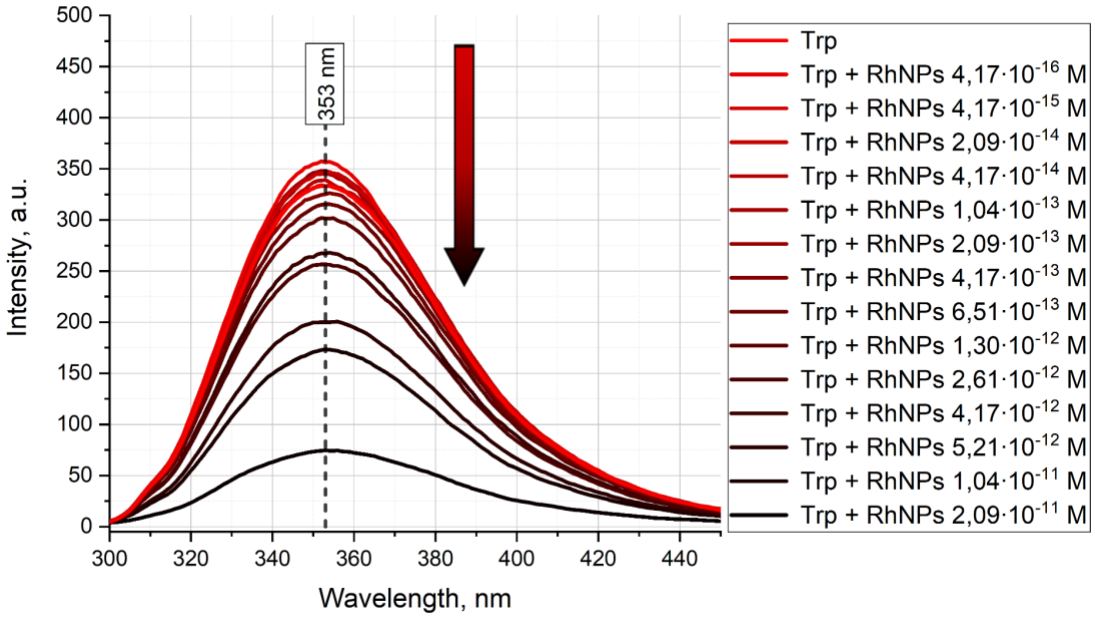


Figure 5. Fluorescence spectra of Trp in the presence of RhNPs with different concentrations. Bright red spectrum-spectrum of Trp without RhNPs, black spectrum - spectrum of Trp with RhNPs of highest concentration ( 2,09 · $10^{-11}$ M).

The fluorescence intensity of Trp decreases almost sevenfold with increasing concentration of RhNPs. The fluorescence maximum occurs at a wavelength of 353 nm and does not change its position.

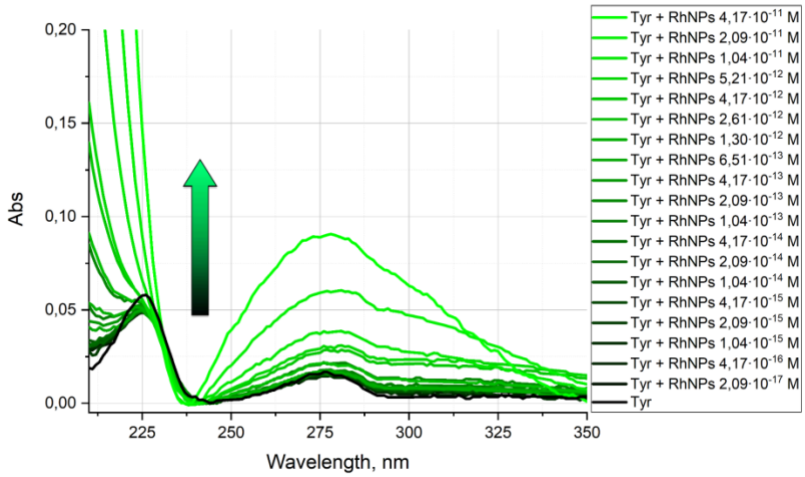


Figure 6. Absorption spectra of Tyr with RhNPs of different concentration. Black spectrum - spectrum of Tyr without RhNPs, bright green spectrum-spectrum of Try with RhNPs of highest concentration ( 2,09 · $10^{-11}$ M).

The absorption of Tyr increases with increasing concentration of RhNPs. The absorption maxima occur at a wavelengths of 220 nm and 275 nm. The positions of the maxima do not change throughout the experiment.

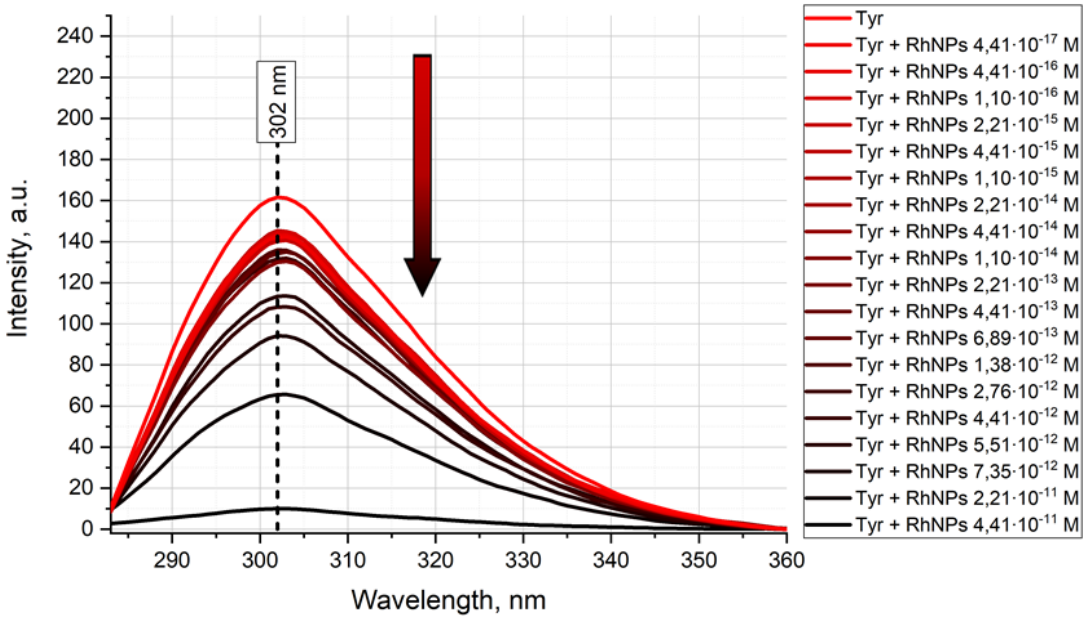


Figure 7. Fluorescence spectra of Tyr in the presence of RhNPs with different concentrations. Bright red spectrum-spectrum of Tyr without RhNPs, black spectrum - spectrum of Tyr with RhNPs of highest concentration ( 4,41· $10^{-11}$ M).

The fluorescence intensity of Tyr decreases almost 16 times with increasing concentration of RhNPs. The fluorescence maximum occurs at a wavelength of 302 nm and does not change its position.

In order to identify the mechanisms of Trp and Tyr fluorescence quenching by RhNPs Stern-Volmer dependencies (Figure 8) were plotted. Each fluorescence spectrum was integrated to calculate the area under the curve to construct a more accurate dependence of fluorescence intensity. The decay kinetics of the excited state of the both amino acids were recorded (Table 1) and also used to determine the mechanisms.

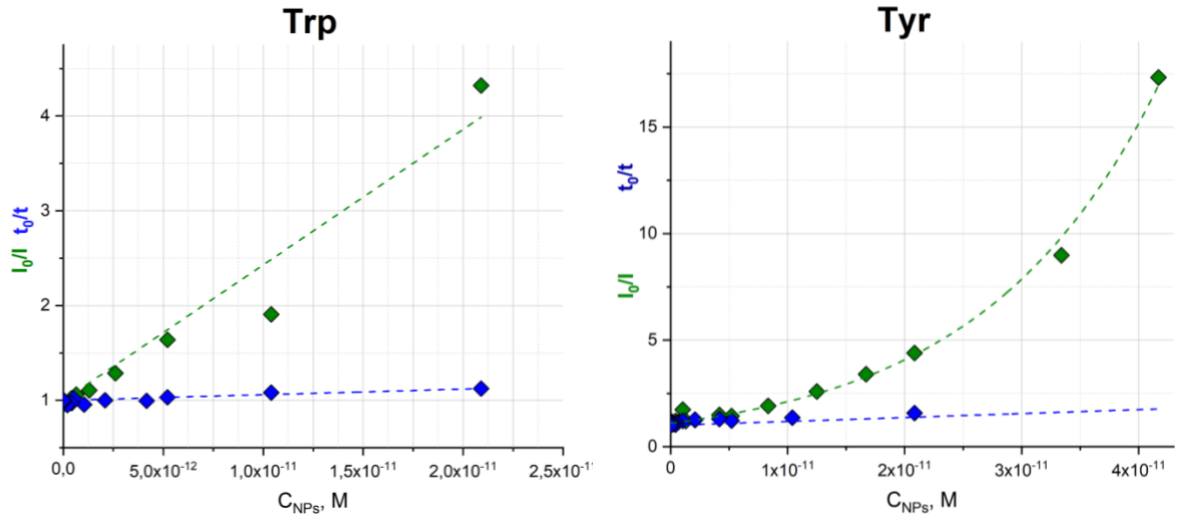


Figure 8. Stern-Volmer plots for the systems: (a) Trp + NPs and (b) Tyr + NPs, where $I_0$, $I$ $(t_0,t)$ denote integral fluorescence intensities (lifetime) of aromatic amino acids in the

absence and presence of quencher.

Lifetimes of each aromatic amino acids in the presence of RhNPs were measured. It was determined that Trp fluorescence lifetime was practically unchanged and the average value was equal to 2.6 ns. Tyr fluorescence lifetime decreased linearly with RhNPs concentration increase and was in the range of values 3.14 - 1.99 ns (see Table 2).

Table 2. Time resolved characteristics for Rh NPs-Tyr/Trp complexes.

| $C_{NPS}$, M | Lifetime,ns* | |
|---|---|---|
| | Trp | Tyr |
| 0 | 2,63 | 3,14 |
| $4{,}4\cdot10^{-15}$ | 2,62 | 2,93 |
| $4{,}4\cdot10^{-14}$ | 2,65 | 2,99 |
| $2{,}2\cdot10^{-13}$ | 2,77 | 2,96 |
| $4{,}4\cdot10^{-13}$ | 2,71 | 3,02 |
| $5{,}5\cdot10^{-13}$ | 2,58 | 2,8 |
| $1{,}1\cdot10^{-12}$ | 2,75 | 2,58 |
| $2{,}2\cdot10^{-12}$ | 2,63 | 2,47 |
| $4{,}4\cdot10^{-12}$ | 2,64 | 2,41 |
| $5{,}5\cdot10^{-12}$ | 2,55 | 2,57 |
| $1{,}1\cdot10^{-11}$ | 2,43 | 2,3 |
| $2{,}2\cdot10^{-11}$ | 2,34 | 1,99 |

*The measurement error for TCSPC measurements was ± 0.1 ns for Tyr and ± 0,06 ns for Trp.

As can be seen from Figure 4(a) Trp lifetime $t$ does not practically change with increasing RhNPs concentration, while its inverse fluorescence relative intensity $\frac{I_0}{I}$ linearly increases, which provided evidence of a static quenching mechanism (ground state complex formation model). In this connection, Coulomb interaction results in non-fluorescent complexes formation between a Trp and negative charged RhNPs. The number of such complexes increases with the quencher concentration raise. The association constant was calculated according to formula (1):

$$\frac{I_0}{I} = 1 + K_s[Q] \quad (1)$$

where $[Q]$ denotes concentration of quencher, $K_s$ is an association constant, which can be estimated as a slope of $(I_0/I - 1)$ vs [Q] graph. The association constant was found to be $1.73 \cdot 10^{11}$ $M^{-1}$ for Trp+RhNPs system.

As can be seen from Figure 4(b), the dependence of lifetime ratios $\frac{t_0}{t}$ for the Tyr+RhNPs system is linear and increases with RhNPs concentration increase. Dependence of fluorescence

intensity ratio $\frac{I_0}{I}$ is non-linear. Deviation from linearity for the obtained dependencies showed that Stern-Volmer model is not optimal for describing the fluorescence quenching within static mechanism and can indicate the simultaneous existence of both static and dynamic quenching mechanism in the Tyr-RhNPs system. In this case, fluorescence quenching occurs due to the formation of nonfluorescent complexes of the amino acid with RhNPs and diffuse collision between tyrosine molecules and RhNPs. The modified form of the Stern-Volmer equation for combined quenching is a second-order equation, which accounts for the upward curvature of the line characteristic of the combined quenching mechanism (2):

$$\frac{I_0}{I} = (1 + K_D[Q])(1 + K_s[Q]) \quad (2)$$

The contribution of dynamic $K_D$ quenching was determined using a linear approximation of the lifetime ratios from equation (3):

$$\frac{t_0}{t} = 1 + K_D[Q] \quad (3)$$

The slope coefficient of the straight line determined the value of the dynamic quenching constant and was equal to $K_D = 3{,}05 \cdot 10^{10}$ $M^{-1}$. The value of the dynamic extinguishing constant was used to estimate the static extinguishing constant in equation (2) and $K_s = 7{,}5 \cdot 10^{10}$ $M^{-1}$.

In addition, the following parameters of quenching efficiency were calculated: diffusion coefficient, diffusion rate parameter, quenching activation energy. Since the size of the quencher (RhNPs) and the fluorophore (Tyr or Trp) differed by an order of magnitude, the calculation formulas were determined as follows.

The diffusion coefficient was calculated using the formula (4):

$$D = \frac{k_B T}{6\pi\eta R} \quad (4)$$

where $k_B$ denotes the Boltzmann constant ($1{,}38 \cdot 10^{-23}$ J/K), T is the temperature, η is the viscosity, R is the RhNPs radius.

The experiment was carried out at T = 20 ◦C. After centrifugation, removal of the supernatant and dilution of the precipitate, the amount of PVP in the precipitate became negligible, thus eliminating its influence on the experiment therefore η = 1,005 was used to determine the diffusion coefficient. The deffusion coefficient was equal to $4{,}03 \cdot 10^{-12}$ $m^2$/sec.

Diffusion rate parameter was calculated using the formula (5):

$$K = \frac{4\pi RDN}{1000} \quad (5)$$

where N is Avogadro's number ($6{,}02 \cdot 10^{23}$ $M^{-1}$). The diffusion rate constant was equal to 1616,84 $m^3$ /sec·M

The activation energy was calculated using the Arrhenius equation (6):

$$K = A \cdot exp^{-\frac{E_a}{RT}} \quad (6)$$

where A is the multiplier, $E_a$ is the activation energy, R is the gas constant (8,31 J/M·K). The viscosity of water was indicated in the temperature range of 5-55 °C every 5 degrees and the corresponding parameters were calculated. All information you can find from Table 3.

Table 3. Parameters of quenching efficiency.

| T, ◦C | T, K | η, mPa·sec | D · $10^{-15}$, $m^2$/sec | K, $m^3$ /sec·M | ln(K) | 1/T |
|---|---|---|---|---|---|---|
| 5 | 278,15 | 1,519 | 2,53 | 1,01 | 6,92264 | 0,003595 |
| 10 | 283,15 | 1,308 | 2,99 | 1,20 | 7,090009 | 0,003532 |
| 15 | 288,15 | 1,14 | 3,49 | 1,40 | 7,244984 | 0,00347 |
| 20 | 293,15 | 1,005 | 4,03 | 1,62 | 7,388228 | 0,003411 |
| 25 | 298,15 | 0,8937 | 4,61 | 1,85 | 7,522513 | 0,003354 |
| 30 | 303,15 | 0,8007 | 5,23 | 2,10 | 7,649028 | 0,003299 |
| 35 | 308,15 | 0,7225 | 5,90 | 2,36 | 7,768156 | 0,003245 |
| 40 | 313,15 | 0,656 | 6,60 | 2,65 | 7,880808 | 0,003193 |
| 45 | 318,15 | 0,5988 | 7,35 | 2,95 | 7,987882 | 0,003143 |
| 50 | 323,15 | 0,5494 | 8,13 | 3,26 | 8,089576 | 0,003095 |
| 55 | 328,15 | 0,5064 | 8,96 | 3,59 | 8,186431 | 0,003047 |

As a result, Figure 9 was plotted and the -$E_a$/R was estimated as a slope of ln(K) vs (1/T). The activation energy was calculated as 19 080,5 J/mol or ≈19 kJ/M.

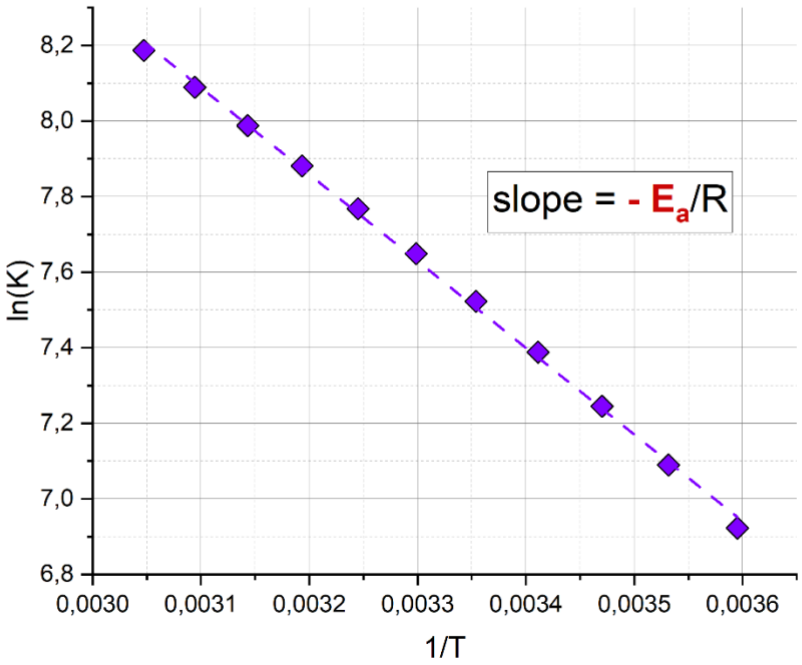

Figure 9. Dependency of ln(K) versus 1/T.

It is worth noting that quenching can also occur as a result of the overlap between the absorption spectrum of the quencher and the fluorescence spectrum of the donor. The size of the NPs and the geometrical arrangement of the donor and acceptor influence the energy transfer mechanism. The close proximity of two molecules (or two parts of a molecule) can lead to an overlap in the electronic state functions of the molecules. In this region, the electrons of the molecules are indistinguishable, which can lead to two-way electron exchange. Such energy transfer occurs in an exchange resonance manner (charge (electron) energy transfer mechanism) [44] (Dexter's mechanism). Realisation of the exchange-resonance mechanism of energy transfer occurs in the near field at small distances between the donor and acceptor, which usually does not exceed 1 nm [45]. Another transport mechanism is inductive resonance energy transfer (dipole-dipole energy transfer (FRET)). The Forster model explains the mechanism of energy transfer between distant molecules at such a distance that no overlapping of electron orbitals occurs. The Ferster mechanism is based on the long-range dipole-dipole Coulomb interaction between electrons or excited donor molecule and acceptor molecule, initially in the ground state, using the coupling of their respective transition dipole moments [45].

Energy transfer can be described by nanometal surface energy transfer (NSET) [46,47]. In the case of NSET, the PM is considered as a two-dimensional (2D) dipole array [48] is a nanosurface having many single dipoles. This transition from a one-dimensional dipole to a two-dimensional dipole array, occurs due to the small size of the NPs, on the order of < 80 nm [46,49,50], where surface and volume are indistinguishable. As is known, the energy transfer rate is related to the donor-acceptor interaction. The key point is that, unlike FRET, NSET does not require a resonant electronic transition. The process of energy transfer via NSET arises from the interaction of the electromagnetic field of the donor dipole with the free conduction electrons of the host metal [51]. In this theoretical model it is assumed that the field reflected from the surface is negligibly small and does not interfere with the dipole field [52], and also does not depend on the size, shape of nanoparticles and the degree of spectral overlap between the donor and acceptor [53]. The inclusion of size dependence in NSET was proposed in the Chance, Prock and Silby-Kuhn (CPS-Kuhn) model, which is discussed below. According to the literature, the process of quenching of fluorophore emission is usually described by FRET, NSET, G-N, and CPS - Kuhn models. To summarise, we assume NSET quenching in the investigated complexes and this model will be tested in our further studies.

Since there are no data on the use of rhodium nanoparticles with proteins, it is possible to assume the possibility of using such particles in transport proteins, such as HSA [54]. In this case, the nanoparticle can be embedded in the binding centres of the protein [55], thus changing its conformation and photophysical properties. The structure of HSA contains several metal binding sites. These binding sites play an important role in the transport of metal ions during certain physiological or pathological processes in vivo, allowing the reversible binding of various metal ions. The existence of these metal binding sites has led to extensive research on HSA as a template for the synthesis of inorganic metal nanomaterials, including silver sulphide (Ag2S), gadolinium oxide (Gd2O3), manganese dioxide (MnO2) and copper sulphide (CuS) [56]. The results obtained in this article demonstrate the possibility of controlling photophysical processes in nanosytems, as well as the prospects for the application of such systems in biophysics.

## Conclusions

RhNPs with a hydrodynamic radius of 53 nm and plasmonic absorption in the UV range have been synthesized. Trp and Tyr fluorescence spectra and decay kinetics in the presence of RhNPs have been recorded. It was shown that static quenching of Trp fluorescence takes place in Trp + RhNPs system while Tyr fluorescence is quenched by RhNPs due to dual mechanisms. Parameters of quenching efficiency: diffusion coefficient, diffusion rate parameter and quenching activation energy were calculated. At present there are known works with quenching of fluorescence of amino acids with other metals, for example, with silver and gold. Researchers are also investigating complexes based on such nanoparticles, for example [38]. However, since the plasmonic maximum of silver and gold is in the visible region, researchers apply FRET-based models to calculate the energy transfer in this case. In our case, the NSET model is assumed in the case of quenching, while the PIRET model is assumed in the case where enhancement would be observed. The addition of metal-containing compounds and nanoparticles can alter the photophysical properties of the complex through the effects of quenching and fluorescence enhancement. The use of rhodium nanoparticles for such applications may be useful for isolating a specific fluorescent protein in urine, selectively binding to it and then quenching it. It is also possible to modify the nanoparticles with specific linkers, for example to the P2Y12 receptors on platelets, and evaluate the conformation of its receptor environment. The main idea for possible future applications of rhodium nanoparticle-based nanosystems is the spectral overlap described above. This provides an opportunity to exploit quenching mechanisms to realise optical sensing effects in UV.

**Funding**

E.D. and A.Z. were supported by the Ministry of Science and Higher Education of the Russian Federation (Agreement Nr. 075-02-2024-1430). I.S. and Al.Z. were supported from the Ministry of Science and Higher Education of the Russian Federation (FZWM-2024-0010).

**Conflict of interest**

Authors state no conflict of interest.

## References


1. S. Basak, K. Chattopadhyay, *Phys. Chem. Chem. Phys*., **2014**, 16, 11139.
2. M.C. Murphy, I. Rasnik, W. Cheng, T.M. Lohman, T. Ha, *Biophysical Journal,* **2004**,86, 2530–2537
3. C.A. Royer, *Chem. Rev*. **2006**, 106, 1769–1784
4. J.T. Vivian, P.R. Callis, *Biophysical Journal*, **2001,** 80, 2093–2109.
5. A. Biswas, R.K. Swarnkar, B. Hussain, S.K. Sahoo, P.I. Pradeepkumar, G.N. Patwari, R. Anand, J. *Phys. Chem. B*, **2014**, 118, 10035–10042.
6. A. Ghisaidoobe, S. Chung, *IJMS* , **2014**, 15, 22518–22538.
7. M. Clerici, G. Colombo, F. Secundo, N. Gagliano, R. Colombo, N. Portinaro, D. Giustarini, A. Milzani, R. Rossi, I. Dalle-Donne, **2014**, 52, 166–174.
8. J.R. Lakowicz, Principles of Fluorescence Spectroscopy, Spinger: Berlin/Heidelberg, Germany, **2006**.
9. Y. Chen, M.D. Barkley, *Biochemistry*, **1998,** 37, 9976–9982.
10. F.W.J. Teale, *Biochemical Journal, **1960**,* 76, 381–388.
11. J. Steinhardt, J. Krijn, J.G. Leidy, *Biochemistry*, **1971**, 10, 4005–4015.
12. R.W. Cowgill, *Biochimica et Biophysica Acta (BBA)-Protein Structure*, **1968**, 168, 417–430.
13. N.G. Zhdanova, E.G. Maksimov, A.M. Arutyunyan, V.V. Fadeev, E.A. Shirshin, *Spectrochimica Acta Part A: Molecular and Biomolecular Spectroscopy*, **2017**, 174, 223–229.
14. M.A. Rub, J.M. Khan, A.M. Asiri, R.H. Khan, K., *Journal of Luminescence, **2014**,* 155, 39–46.
15. R. Li, D. Dhankhar, J. Chen, T.C. Cesario, P.M. Rentzepis, *Proc. Natl. Acad. Sci. U.S.A.* , **2019**, 116, 18822–18826.
16. E. Demishkevich, A. Zyubin, A. Seteikin, I. Samusev, I. Park, C.K. Hwangbo, E.H. Choi, G.J. Lee, *Materials,* **2023,** 16, 3342.
17. Y. Jeong, Y.M. Kook, K. Lee, W.-G. Koh, *Biosensors and Bioelectronics*, **2018**, 111, 102–116.
18. K. Aslan, I. Gryczynski, J. Malicka, E. Matveeva, J.R. Lakowicz, C.D. Geddes , *Current Opinion in Biotechnology*, **2005**, 16, 55–62.
19. T. Ribeiro, C. Baleizão, J.P.S. Farinha, *Sci Rep*, **2017**, 7, 2440.
20. J.-H. Choi, J.-W. Choi, *Nano Lett*., **2020**, 20, 7100–7107.
21. J. Chen, Y. Jin, N. Fahruddin, J.X. Zhao, *Langmuir*, **2013**, 29, 1584–1591.
22. B. Della Ventura, M. Gelzo, E. Battista, A. Alabastri, A. Schirato, G. Castaldo, G. Corso, F. Gentile, R. Velotta, *ACS Appl. Mater. Interfaces*, **2019**, 11, 3753–3762.
23. K. Aslan, S.N. Malyn, C.D. Geddes, *J Fluoresc*, **2006**, 17, 7–13.
24. K. Aslan, J.R. Lakowicz, C.D. Geddes, *Anal Bioanal Chem*, **2005**, 382, 926–933.
25. M.H. Chowdhury, K. Ray, S.K. Gray, J. Pond, J.R. Lakowicz, *Anal. Chem*., **2009**, 81, 1397–1403.
26. J.M. McMahon, G.C. Schatz, S.K. Gray, *Phys. Chem. Chem. Phys*., **2013**, 15, 5415–5423.
27. Y. Zhang, K. Aslan, M.J.R. Previte, C.D. Geddes, *Applied Physics Letters*, **2007**, 90, 173116.
28. M.W. Knight, N.S. King, L. Liu, H.O. Everitt, P. Nordlander, N.J. Halas, *ACS Nano,* **2014***,* 8, 834–840.
29. Y. Gutierrez, D. Ortiz, J.M. Sanz, J.M. Saiz, F. Gonzalez, H.O. Everitt, F. Moreno, *Opt. Express*, **2016**, 24, 20621.
30. Y. Gutiérrez, R. Alcaraz De La Osa, D. Ortiz, J. Saiz, F. González, F. Moreno, *Applied Sciences*, **2018**, 8, 64.
31. N. Akbay, F. Mahdavi, J.R. Lakowicz, K. Ray, *Chemical Physics Letters*, **2012**, 548, 45–50.

32. C.-S. Chu, T.W. Sung, Y.L. Lo, *Sensors and Actuators B: Chemical*, **2013,**185, 287–292.
33. D. Ghosh, N. Chattopadhyay, *Journal of Luminescence*, **2015**, 160, 223–232.
34. C. Hao, G. Xu, Y. Feng, L. Lu, W. Sun, R. Sun, *Spectrochimica Acta Part A: Molecular and Biomolecular Spectroscopy*, 2017, 184, 191–197.
35. K.A. Kang, J. Wang, J.B. Jasinski, S. Achilefu, *J Nanobiotechnol*, **2011**, 9, 16.
36. P. Anger, P. Bharadwaj, L. Novotny, *Phys. Rev. Lett.*, **2006**, 96,113002.
37. A.M. Queiroz, A.V. Mezacasa, D.E. Graciano, W.F. Falco, J.-C. M'Peko, F.E.G. Guimarães, T. Lawson, I. Colbeck, S.L. Oliveira, A.R.L. Caires, *Spectrochimica Acta Part A: Molecular and Biomolecular Spectroscopy*, **2016**, 168, 73–77.
38. S. Roy, T.K. Das, *J Appl Spectrosc*, **2015**, 82, 598–606.
39. B.P. Espósito, A. Faljoni-Alário, J.F.S. De Menezes, H.F. De Brito, R. Najjar, *Journal of Inorganic Biochemistry*, **1999**, 75, 55–61.
40. M.Z. Bellus, M. Li, S.D. Lane, F. Ceballos, Q. Cui, X.C. Zeng, H. Zhao, *Nanoscale Horiz.,* **2017***,* 2, 31–36.
41. S. Kundu, K. Wang, H. Liang, *J. Phys. Chem*., **2009**, 113, 18570–18577.
42. T. Wakita, H. Yao, *Chemical Physics Letters*, **2021**, 779,138866.
43. G. Kumar, R.K. Soni, *J Raman Spectroscopy*, **2022**, 53, 1890–1903.
44. D.L. Dexter, A Theory of Sensitized Luminescence in Solids, *The Journal of Chemical Physics*, **1953**, 21, 836–850.
45. H.V. Demir, S.V. Gaponenko, Applied Nanophotonics, *Cambridge University Press*, **2018**.
46. C.S. Yun, A. Javier, T. Jennings, M. Fisher, S. Hira, S. Peterson, B. Hopkins, N.O. Reich, G.F. Strouse, *J. Am. Chem. Soc*. **2005**, 127, 3115–3119
47. P.F. Gao, Y.F. Li, C.Z. Huang, *TrAC Trends in Analytical Chemistry*, **2020**, 124, 115805.
48. S. Rakshit, S.P. Moulik, S.C. Bhattacharya, *Journal of Colloid and Interface Science*, **2017**, 491, 349–357.
49. T.L. Jennings, J.C. Schlatterer, M.P. Singh, N.L. Greenbaum, G.F. Strouse, *Nano Lett*., **2006**, 6, 1318–1324.
50. M.P. Singh, G.F. Strouse, *J. Am. Chem. Soc*, **2010**, 132, 9383–9391.
51. T. Sen, S. Sadhu, A. Patra, *Applied Physics Letters*, **2007**, 91, 043104.
52. C. Chen, N. Hildebrandt, Resonance energy transfer to gold nanoparticles: NSET defeats FRET, TrAC Trends in Analytical Chemistry 123 (2020) 115748.
53. C.J. Breshike, R.A. Riskowski, G.F. Strouse, Leaving Förster Resonance Energy Transfer Behind: Nanometal Surface Energy Transfer Predicts the Size-Enhanced Energy Coupling between a Metal Nanoparticle and an Emitting Dipole, J. Phys. Chem. C 117 (2013) 23942–23949.
54. K. Bolaños, M.J. Kogan, E. Araya, Capping gold nanoparticles with albumin to improve their biomedical properties, IJN Volume 14 (2019) 6387–6406.
55. W. Bal, M. Sokołowska, E. Kurowska, P. Faller, Binding of transition metal ions to albumin: Sites, affinities and rates, Biochimica et Biophysica Acta (BBA) - General Subjects 1830 (2013) 5444–5455.
56. H. Iqbal, T. Yang, T. Li, M. Zhang, H. Ke, D. Ding, Y. Deng, H. Chen, Serum protein-based nanoparticles for cancer diagnosis and treatment, Journal of Controlled Release 329 (2021) 997–1022.